AGU ADVANCING EARTH AND SPACE SCIENCE

Water Resources Research

RESEARCH ARTICLE
10.1029/2020WR029457

Intraseasonal-to-Interannual Analysis of Discharge and Suspended Sediment Concentration Time-Series of the Upper Changjiang (Yangtze River)

C. Juez[1], N. Garijo[2], M. A. Hassan[3], and E. Nadal-Romero[1]

[1]Instituto Pirenaico de Ecología, Consejo Superior de Investigaciones Científicas (IPE-CSIC), Zaragoza, Spain, [2]Centro Universitario de la Defensa, Zaragoza, Spain, [3]Department of Geography, The University of British Columbia, Vancouver, BC, Canada

Key Points:

- Distinct time-scales of discharge and suspended sediment concentration (SSC) are identified and related qualitatively to seasonal, annual, and short (1.1–5 years) and long-term (5.5–20 years) variability
- Similar dominant time-scales of variability for discharge and SSC are identified in the Upper Changjiang for a 50-year study period
- Bi-modal seasonal climatic pattern influence short-term time-scales whereas high magnitude flow events control intra-annual time-scales

Supporting Information:

Supporting Information may be found in the online version of this article.

Correspondence to:

C. Juez,
carmelo.juez@ipe.csic.es

Citation:

Juez, C., Garijo, N., Hassan, M. A., & Nadal-Romero, E. (2021). Intraseasonal-to-interannual analysis of discharge and suspended sediment concentration time-series of the Upper Changjiang (Yangtze River). *Water Resources Research*, *57*, e2020WR029457. https://doi.org/10.1029/2020WR029457

Received 21 DEC 2020
Accepted 15 JUL 2021

Abstract Sediment transport is the main driver of the channel morphology and landscape evolution, with implications for chemical and biological river processes, and human-related activities. Understanding the processes governing the relations between discharge and suspended sediments is essential for the management of river catchments and river networks. Here, we use the method of wavelet transformation to identify the time-scale dependency of suspended sediment patterns concerning the temporally and spatially uneven transient processes of sediment production, accumulation, and transport. We analyze the temporal variation of concurrent discharge and suspended sediment fluxes for the Upper Changjiang (Yangtze River, China) at Pingshan station by using a long-term database collected for over 50 years. Furthermore, we bridge the limitations of pure predictive models to learn from temporal data structures with the main purpose of identifying the mechanisms underpinning the suspended sediment patterns (e.g., climatic forces). Intraseasonal-to-seasonal, annual, and inter-annual dominant time-scales are thus identified. The short time-scales are driven by the bi-modal seasonal precipitation pattern specific to the climate of the region and provide a continuous supply of sediments to the river. The large time-scales, controlled by high magnitude flow events and within-reach sediment storage, display alternating periods of increasing and decreasing sediment fluxes; ultimately, they maintain the river channel within balance or within a moderate positive sediment accumulation process. This analysis and methodology help to understand temporal sediment dynamics, and ultimately to manage river catchments.

1. Introduction

Suspended sediment load comprises the major portion of the total clastic load in most rivers (e.g., Rhoads, 2020 see summary table 3.1) and is an important component for understanding channel dynamics and landscape evolution. In addition, suspended sediment is a major component of the biological, physical, and chemical processes in rivers (Matos et al., 2018). In river environments, suspended, or "fine" sediment is typically defined as clasts or organic material finer than 0.2 mm and is widely recognized as a leading pollutant within river systems (e.g., Rhoads, 2020). Understanding the suspended sediment dynamics is important for assessing how the climate and land use impact drainage basins. Beyond river geomorphology and landscapes, better understanding of suspended sediment processes is also critical for a range of fluvial processes, including nutrients and pollutants transport (Baxter & Hauer, 2000; De Vries & Klavers, 1994; Horowitz, 1995; Horowitz et al., 2001; Sternecker et al., 2013), sustainability of human infrastructure (Schleiss et al., 2016), overbank sedimentation (Juez et al., 2019), or catchment-level fluxes of carbon (Boix-Fayos et al., 2015). Furthermore, knowledge of fine sediment sources, transport, and deposition is prerequisite for sediment load predictions, development of land use policy and making appropriate land management decisions. Although fine sediment dynamics has been the focus of many studies, the current knowledge of sediment sources transfer and storage is inadequate to address the wide environmental significance of fine sediment dynamics in the landscape.

Suspended sediment transport is primarily controlled by flow discharge characteristics (magnitude, duration, and turbulence) and the settling velocity of the grains which largely depends on the submerge weight of the grain (e.g., Chien & Wan, 1999; Rhoads, 2020; Rijn, 1984). Power law relations between suspended sediment concentration (SSC) and flow discharge were developed and used to estimate fine sediment load.

Because of the large scatter in the data, power relations yielded to large errors in the estimation of sediment load for most field cases (Ashworth & Ferguson, 1986; Walling, 1977; Walling & Webb, 1981, 1988). These relations tend to underestimate loads for relatively high flows (Gao, 2008; Horowitz, 2003) and to overestimate the load for low flows (Horowitz, 2003) resulting in substantial error in the estimation of seasonal or annual load (Horowitz, 2003). An estimated error of concentration-discharge relation ranging between 14% and 73% has been reported in the literature (Phillips et al., 1999; B. P. G. Smith et al., 2003a, 2003b; Webb et al., 1997). Thereby, these relations perform well only for relatively small basins with homogeneous conditions (Gao et al., 2013). To improve the performance of sediment concentration-flow relations, alternative statistical methods have been suggested including generalize linear models (Cox, 2008), and the logarithmic transform data and power function based on nonlinear least square method (Asselman, 2000). Patil et al. (2012) and S. M. C. Smith et al. (2013) pointed out that relations between sediment load and discharge are nonlinear, implying that even small errors in sediment or flow inputs will likely result into a large error in predicting the sediment load.

Although estimating fine sediment transport as a function of flow characteristics has been explored extensively for few decades, predicting sediment load using concentration-discharge relations remains challenging. Regardless of the size of the basin, large body of research has shown that fine sediment transport is largely controlled by the sediment supply from both external and internal sources of sediment (e.g., Rhoads, 2020; Salant et al., 2008). External sediment supply sources from the landscape include mass movements, gully and rill erosion, and surface runoff of exposed soil. Stream bed and banks are the sources of internal fine sediment that include bars, back water areas, pools, banks, and fines from the subsurface and bed interstices (see Lamb et al., 2020). Sediment supply causes hysteresis in the relation between concentration and discharge (i.e., different sediment fluxes are observed for the same discharge on the rising and falling limb of the flow hydrograph). Thereby, the interplay between sediment supply and flow results in the observed complex spatial and temporal distributions of suspended sediment. In other words, the spatial and temporal variation in the production, transport, and deposition of sediment, causes the sediment hysteresis. At a location in the channel (e.g., gauging station), the measured SSC is the integrated input from a wide range of processes that act at different time and spatial scales. The diverse physical mechanisms that influence fine sediment dynamics take place at different time and spatial scales, making them difficult to observe and model especially in large basins (Tsuruta et al., 2018).

To overcome such complexity, some researchers have resorted to machine learning models to predict and forecast spatial and temporal patterns of SSC and load (e.g., Choubin et al., 2018; Kumar et al., 2015; Matos et al., 2018). Relying on learning from the data structure, machine learning models approximate/forecast unknown, nonlinear, and multidimensional laws from observed data with little representation of the physical processes underlying the phenomena of interest. For instance, Matos et al. (2018) investigated a long suspended sediment data set measured simultaneously with discharge at Pingshan station in the Upper Changjiang (Yangtze River) to forecast and predict suspended sediment dynamics. Following a machine learning strategy, these authors developed a probabilistic forecasting model able to predict temporal patterns in the observed data. However, two main shortcomings are associated with this methodology: (a) these techniques should only be applied to a statistically stationary time-series. Forecasted results depend heavily on the training subsets chosen. Thus, if the time-series displays high temporal variability (e.g., a declining trend from a certain point in the series or episodic events with varying magnitude occurring at different and non-similar time-scales), the reliability of the predicted results are compromised since the training subsets may not be representative of the data set; (b) these methods work as a black-box, which implies that learning about the physical processes driving the time-series dynamics through a direct view of the predicted results is complicated or even impossible. Machine learning develops a model based on the temporal structure of some of the observations (training subsets) but with little physical guidance. This model is then used to predict the temporal pattern of the remaining observations. The comparison with predictions is thus an evaluation of how well the temporal structure captured by the model can be generalized beyond the training observations. However, this methodology cannot decompose the temporal structure of the data in several levels or time-scales and as such, the transient physical processes driving the dynamics of the time-series are not time-localized/identified or even the selected training subsets are not relevant within the data temporal structure. In other words, without identifying and localizing the dominant time-scales, the training of the machine learning model may be flawed and unsuccessful.

The objective of this study consists of bridging the limitations of pure predictive models in order to learn from temporal data structures with the main purpose of characterizing and better understanding the mechanisms underpinning the suspended sediment patterns. We aim at unraveling the time-scales dependency of the sediment patterns with regard to the temporally and spatially uneven transient processes of sediment production, storage and transport. This point is even more challenging in a large catchment where: (a) the time-series include information of a complex integration of sediment processes (e.g., accumulation or removal of sediment on the streambed, banks, and floodplain), and (b) the temporal and spatial trends of such sediment processes may be related to land use changes and climatic shifts in the catchment.

To achieve the above goal we use the method of wavelet transformation because of its ability to capture processes variability at multiple time-scales (Torrence & Compo, 1998). The wavelet transform has been successfully applied in the past to a hydro-climatic time-series (Segele et al., 2009; Webster & Hoyos, 2004) and to discharge-precipitation time-series (Carey et al., 2013; Juez & Nadal-Romero, 2020a,2020b) to determine periodicities and trends. We use the wavelet transform instead of other temporal analysis techniques such as Fourier spectral analysis (processes are identified by periodicity, e.g., L. C. Smith et al., 1998) or multi-scale entropy analysis (processes are identified by their degree of complexity or randomness, e.g., Y. Wang et al., 2018) because of their favorable strengths: (a) wavelet transform can identify processes in both time and periodicity in the non-stationary time-series (contrary to Fourier spectral analysis), and (b) wavelet transform allows to localize dominant time-scales within the complete temporal spectrum, ultimately identifying the variability of each time-scale throughout the study period (contrary to Fourier spectral analysis and entropy analysis). The wavelet transform is applied to a long period data set recorded at Pingshan gauging station at the mainstem of the Upper Changjiang. Our analysis encompasses the period 1952–2007. The impact of seasonal, annual, and multi-annual episodic events on SSC time-series and ultimately on the river-reach morphology is thus identified and quantified.

2. The Upper Changjiang Catchment Defined at Pingshan Station

Data used in this study were collected by the Changjiang Commission at Pingshan gauging station within the Upper part of the Changjiang Basin. The Changjiang is the largest river in China with a length of 6,400 km and a total drainage area of 1.94×10^6 km^2. The river flows eastward from its sources in the Dangla Mountain Range in Qinghai Province into the East China Sea (see Figure 1). The Changjiang flow through four major physiographic regions: Qinghai-Tibet Plateau, Sichuan Basin, Changjiang Gorges, and Jianhan Basin (J. Li et al., 2001). The catchment is divided into three parts (see Figure 1): (a) the upper mountainous and hilly part extends from the headwaters to Yichang and drains about 59% of the catchment, (b) the middle refers to the river reach between Yichang and Hankou (draining about 87% of the contributing area), and (c) the lower part is from Hankou to Shanghai (X. Q. Chen et al., 2008; Z. Chen, Li, et al., 2001; Z. Chen, Yu, & Gupta, 2001). The mean temperature increases from 4°C near the headwaters, to 17–20°C in Sichuan catchment and lower parts of the river (Z. Y. Wang et al., 2007). Mean precipitation is 270 mm near the water divides in Tibet Plateau, 870 mm in Sichuan Basin and increased to 1,460 mm in the middle and eastern parts of the basin (Z. Y. Wang et al., 2007). The annual discharge increases downstream from 0.46×10^4 m^3/s at Pingshan to 1.4×10^4 m^3/s at Yichang, 2.3×10^4 m^3/s at Hankou and 2.8×10^4 m^3/s at Datong (see Figure 1) (Z. Chen, Li, et al., 2001; Z. Chen, Yu, & Gupta, 2001; Z. Y. Wang et al., 2007).

Pingshan gauging station is located within the upper part of the Changjiang near the boundary between the Eastern Mountains of the Tibet Plateau and the Sichuan Basin. The contributing area at Pingshan station is about 475,000 km^2. The Plateau of Tibet, which is still being uplifted as the Indian and Eurasian plates collide, composed of igneous, marine sedimentary, and metamorphic rocks with thick deposits of overlying sediments. From the Tibet Plateau, the Changjiang flows through gorges deeply incised into mountainous plateaus consisting of Paleozoic and Mesozoic rocks. Upstream of the Pingshan gauge station, the river is confined and incised into bedrock, forming a deep canyon (Z. Chen, Li, et al., 2001; Z. Chen, Yu, & Gupta, 2001). The channel width, depth and slope range between 500 and 1,500 m, 5–20 m, and $0.1–0.4 \times 10^{-3}$, respectively (Z. Chen, Li, et al., 2001; Z. Chen, Yu, & Gupta, 2001; Hassan et al., 2010). Downstream of Pingshan station, the channel gradient declines significantly (slope ranges between $0.07–0.25 \times 10^{-3}$), and the flow regime and the channel morphology change. East of Pingshan station, the river meanders within a relatively narrow floodplain, with point and mid channel bars dominating the channel morphology.

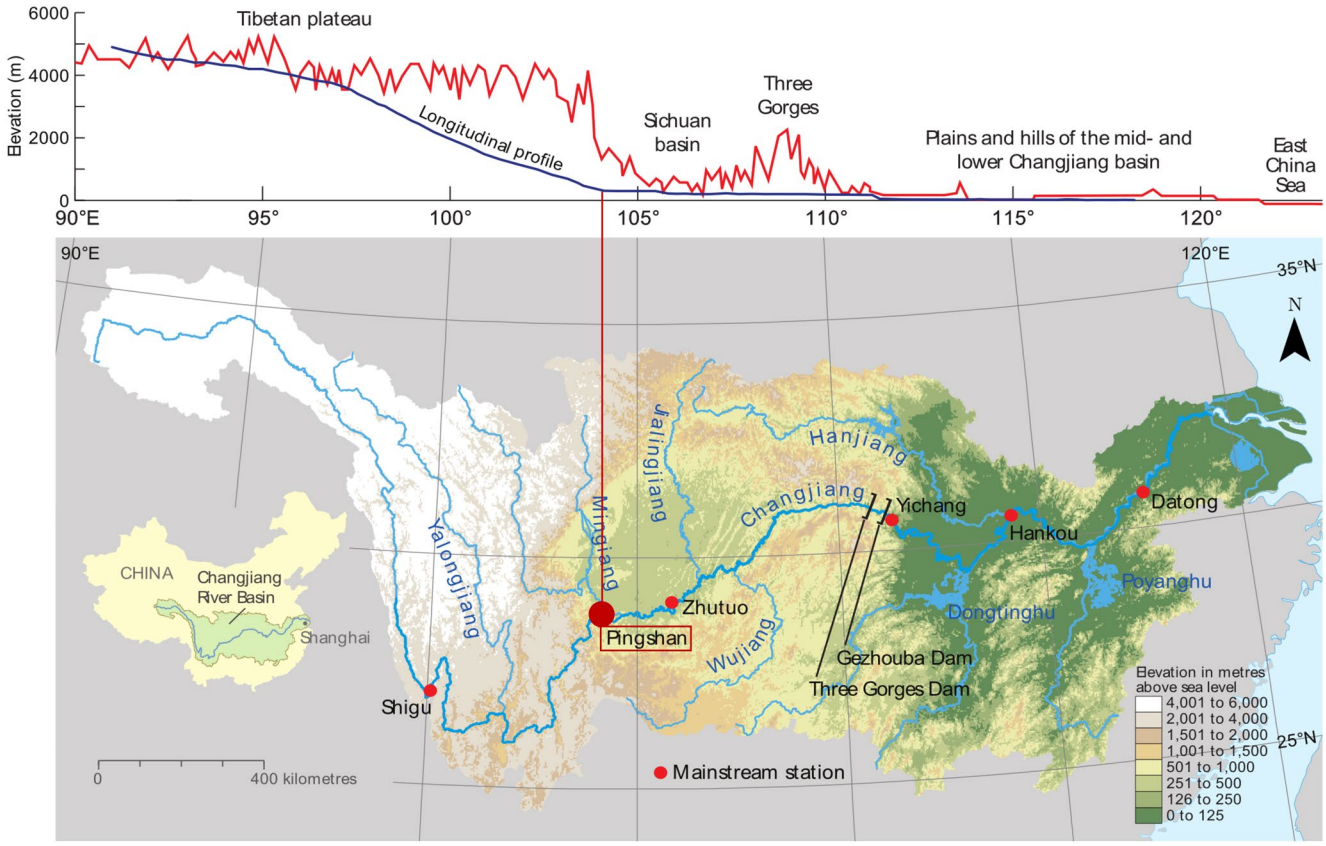

Figure 1. The Changjiang (Yangtze River) catchment, showing the location of the Pingshan station in the Upper Changjiang, the longitudinal profile of the mainstem, the cross section through the catchment geomorphological units (red line), the land topography and the main contributing tributaries along the mainstem of the river, and the two major dams located in the catchment (Gezhouba dam and Three Gorges dam).

Since the 1970s, large changes in land use and soil conservation measures aimed at reducing soil erosion have brought under management large areas of the basin, resulting in a major decline in sediment delivery to the East China Sea (Z. Chen, Li, et al., 2001; Z. Chen, Yu, & Gupta, 2001; Hassan et al., 2010; Lu & Higgitt, 1998, 1999; Walling, 2006; Z. Y. Wang et al., 2007). Hassan et al. (2010, 2011) examined the reach scale suspended sediment budget for the Changjiang. For the Shigu-Pingshan reach (upstream of Pingshan station, see Figure 1), they reported a net degradation for the years 1950–1987. Furthermore, significant changes in the sediment storage were recorded for the years 1965–1968 and 1974 (Hassan et al., 2011). In terms of fine sediment sources into the reach ~25% from upstream, 50%–55% from large and small tributaries, and 20%–25% from landscape adjacent to the mainstem (Hassan et al., 2011). Downstream of Pingshan station, a clear depositional trend was observed for the Pingshan-Zhutuo reach (see Figure 1) for the period (Hassan et al., 2011). The dominance of the aggradation along the reach is because of the dramatic decline in the river channel gradient (see Figure 1) and changes in channel morphology. In contrast to the reach upstream of Pingshan station, for the downstream Pingshan-Zhutuo reach most of the sediment derives either from upstream (~75%) or main tributaries (~20%) (Hassan et al., 2010, 2011). In summary, about 75% of the sediment measured at Pingshan station comes from upstream and the rest comes from Mingiang and other small tributaries (see Figure 1).

For this study, we reviewed the available Land Use and Land Cover (LULC) data from Data Sharing Infrastructure of Earth System Science, National Scientific Data Shared Platform (www.geodata.cn). However, direct links and lags between LULC and sediment yields remain complex due to two major challenges already pointed out by Higgit & Lu (1999): (a) the weak synchrony between sediment records (daily records for 1952–2007) and land use information (scarce digital maps, since 1980 one map each 5–6 years, F. Wang et al., 2013), and (b) the coarse digital map scale resolution (ranging between 1:100,000 and 1:250,000,

F. Wang et al., 2013). Consequently, the temporal decomposition provided by the wavelet decomposition serves as a proxy to infer relationships between LULC changes and sediment dynamics.

3. Data and Methods

3.1. Discharge and Suspended Sediment Load Data

Daily suspended concentration and hydrological gauging data for Pingshan station for the period 1952–2007 were obtained from the Changjiang Commission (Annual reports from Ministry of Water Resources of the People's Republic of China, 1952–2007). Discharge was measured 5–6 times a day and averaged to obtain a mean daily value for the period 1952–2007 through the float method, flowmeters and water level probes. Rating curves were created based on the measurements. The plotted rating curves were relatively stable, and in general, all points of measurement were distributed close to the best-fit curve. Conversely, daily grab samples of suspended sediment are collected regularly at the same location, and load is calculated using the concentration and discharge (Hassan et al., 2010). Sediment samples are collected through bottle samples along 25 verticals (equally cross-section spaced) and are used to calculate the vertical average concentration. At each vertical, between 3 (1952–1960) and 6 (1961–2007) point measurements (equally water-depth spaced) are taken. To better represent the sediment concentration during high flows (floods), the Commission increases the sampling to 5–6 times a day. The sediment contained in the bottle samplers is filtered, dried, and weighed to determine the point localized sediment concentration. Then, the depth-averaged sediment concentration values are obtained based on the point samples. Finally, the depth-averaged sediment concentration measured over cross sections is used to compute the daily cross section averaged value (Hassan et al., 2010). Given that this study is focused on the temporal patterns of suspended sediment collected from the same cross section, we assume that errors associated with the flow discharge and suspended concentration measurements are systematic. A typical error for estimating the annual sediment load falls within about ±10% when the standard deviation of the error for both water and sediments is assumed to be similar (McLean et al., 1999). In the absence of more specific information, we adopt this value for this work as a figure of merit for our analysis (see also Hassan et al., 2010).

Examining the grain size distribution of the suspended sediment at Pingshan station yielded a mean value of 0.044 and 0.021 mm for the periods 1964–1985 and 1956–2007, respectively (Hassan et al., 2010). The decline in the grain size of the suspended sediment was attributed to changes in land use and dam constructions (Z. Y. Wang et al., 2007; Xu, 2007). This implies that most of the time (∼95%) the mobile fine sediment is in the silt-clay grain size range and that the suspended concentration is uniformly distributed within the water volume (see Rhoads, 2020). This is an important assessment to be taken into account since as reported by previous authors in large rivers there is a strong variability of vertical SSC gradients as a function of sediment grain size (see Regüés & Nadal-Romero, 2013; Santini et al., 2019) and also because of flocculation effects (see Lamb et al., 2020).

Non-parametric Mann-Kendall and Pettit tests were preliminary applied to the discharge and SSC time-series to identify possible temporal trends and tipping points. The variations of monthly, seasonal, and annual trends in time were thus analyzed. Both tests show that discharge data do not have any trend statistically significant within the study period (resulting *p*-values were above 0.05 and thus not statistically significant). On the contrary, for SSC data a declining rate (statistically significant) is identified for both tests during the period 1998–2007. The stationarity of discharge time-series along the study period is in agreement with previous research carried out on this area. J. Chen et al. (2014) conducted an analysis of the hydrological changes of the Changjiang river based on runoff, precipitation, and temperature time-series recorded during the period of 1955–2011 (which it is similar to our study period 1952–2007). Results from J. Chen et al. (2014) stated that no statistically significant trend was detected in annual precipitation in the Upper Changjiang catchment using the Mann-Kendall test. More recently, Z. Li et al. (2020), carried out a discharge and sediment concentration analysis during the period of 1985–2016 in the Tuotuohe gauging station, located in a sub-catchment of the Upper Changjiang catchment, within the Tibetan Plateau at approximately 4,500 m.a.s.l and 1,800 km upstream of Pingshan station. Tuotuohe gauging station, dominated by snowfall and melting permafrost, displayed a sustained increased in both discharge and sediment concentration time-series over the study period due to global warming. However, these observations are not

reflected in our data set or in J. Chen et al. (2014) data set. Thus, changes in runoff and discharge due to long-term climatic shifts are not assertively identified in the Upper Changjiang catchment.

3.2. Wavelet Analysis

Discharge and SSC time-series are rarely stationary and they consist of a broad set of transient patterns varying within the temporal record. The wavelet transform allows to localize in both time and periodicity the transient patterns recorded in such non-stationary time-series. It thus provides a complete time-scale representation of localized and transient phenomena occurring at different time-scales (Torrence & Compo, 1998). In this research, we make use of the Morlet wavelet, which was successfully used in the past to analyze precipitation and discharge time-series (Carey et al., 2013; Labat et al., 2005). This wavelet type is characterized as:

$$\varphi_0(\eta) = \pi^{-1/4} e^{i\omega_0\eta} e^{-\eta^2/2} \tag{1}$$

where $\varphi_0(\eta)$ is the wavelet function, η, is a dimensionless time parameter, i is the imaginary unit and ω_0 is the dimensionless angular frequency taken as 6 which provides a right match between time and frequency localization. Thus, for a time-series X_n for each scale s at all n of series length N, the wavelet function is mathematically represented as:

$$W_n(s) = \frac{1}{N} \sum_{n'=0}^{N-1} x_{n'} \psi^* \left[\frac{(\eta' - \eta)\Delta t}{s} \right] \tag{2}$$

where $W_n(s)$ is the wavelet transform coefficients, ψ the normalized wavelet, (*) the complex conjugate, s the wavelet scale, n the localized time index, and n' the translated time index of the time ordinate x.

In addition, to identify the transient time-scales all through the temporal records we also compute the wavelet coherence (Grinsted et al., 2004), which compares two wavelet spectra, discharge and SSC records in our case. The wavelet coherence is similar to the correlation coefficient computed all through the temporal record between two time-series, X and Y, with wavelet transforms $W_n^X(s)$ and $W_n^Y(s)$. The wavelet coherence is computed as:

$$R_n^2(s) = \frac{| S\left(s^{-1} W_n^{XY}(s)\right) |^2}{S\left(s^{-1} | W_n^X(s) |^2\right) \cdot S\left(s^{-1} | W_n^Y(s) |^2\right)} \tag{3}$$

being S a smoothing operator for both scale and time domain.

$$S(W) = S_{\text{scale}}\left(S_{\text{time}}\left(W_n(s)\right)\right) \tag{4}$$

where S_{time} smooths along the scale axis and S_{time} smooths along the time axis. Further details on wavelet coherence analysis are provided in Grinsted et al. (2004).

4. Results

4.1. Temporal Spectrum Analysis

Results displayed in Figures 2–4 allow identifying the dominant time-scales of the transient patterns embedded in the temporal records, based on the amplitude peaks and local wavelet power.

Based on the global and local wavelet power spectrum, non-overlapping dominant time-scales were identified for the largest power peaks. Table 1 thus gives information on what percentage of the data temporal variability is explained by the contribution of each dominant time-scale.

The temporal spectrum analysis of both discharge and SSC time-series features intra-seasonal (0.003–0.6 years), annual (0.9–1.1 years), short-term-annual (1.1–5.5 years), and long-term-annual (5.5–20 years) episodic patterns. In both time-series, the annual cycle (see Table 1) contains the dominant power in both discharge and SSC wavelet spectrum and it accounts itself for the 40% and 46% of the total variance. This is further illustrated in Figure 4, where a notably regular annual periodicity is observed in the discharge and

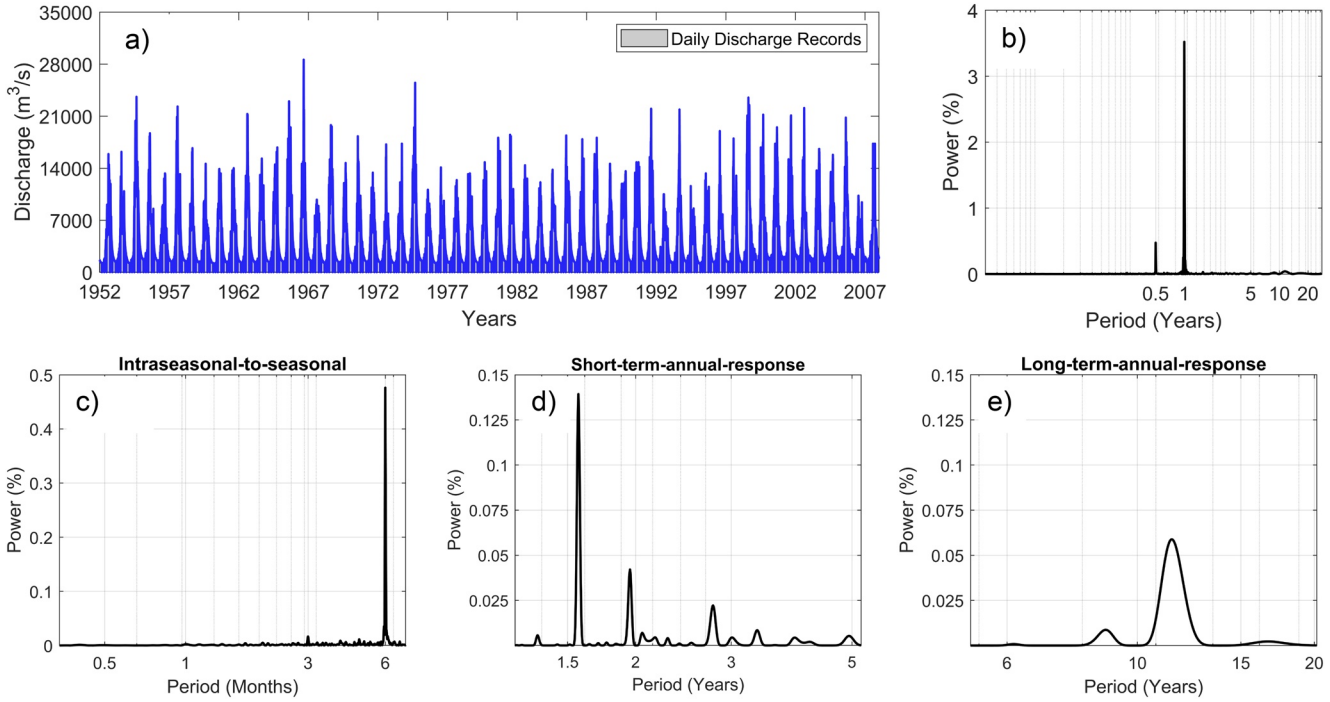

Figure 2. Spectral characteristics of discharge time-series of Changjiang recorded during the period 1952–2007 at Pingshan station. (a) Time-series of daily discharge records; (b) global wavelet periodogram expressed as percentage of total global power summed over all periods. Time-scales beyond the dominant annual time-scale are identified and magnified in the bottom figures; (c) intraseasonal-to-seasonal response; (d) short-term annual response; (e) long-term-annual response.

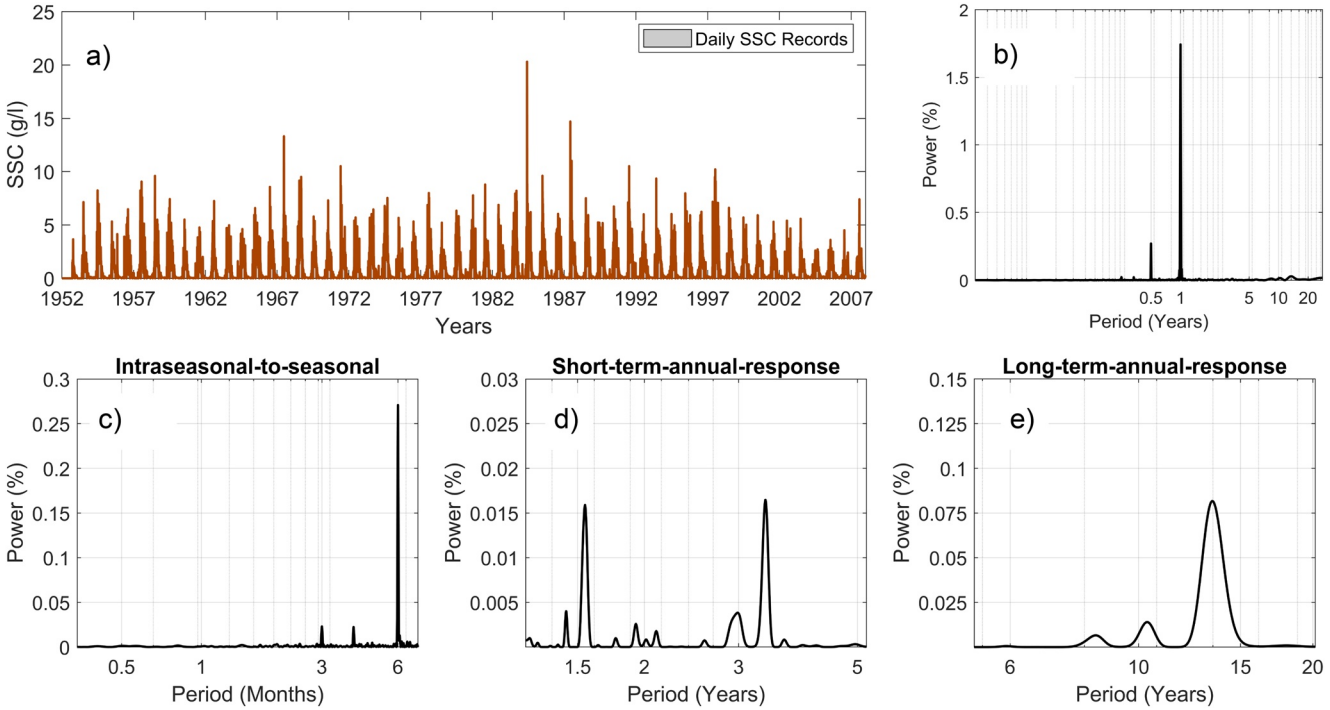

Figure 3. Spectral characteristics of suspended sediment concentration (SSC) time-series of Changjiang recorded during the period 1952–2007 at Pingshan station. (a) Time-series of daily SSC records; (b) global wavelet periodogram expressed as percentage of total global power summed over all periods. Time-scales beyond the dominant annual time-scale are identified and magnified in the bottom figures; (c) intra-seasonal-to-seasonal response; (d) short-term annual response; (e) long-term-annual response.

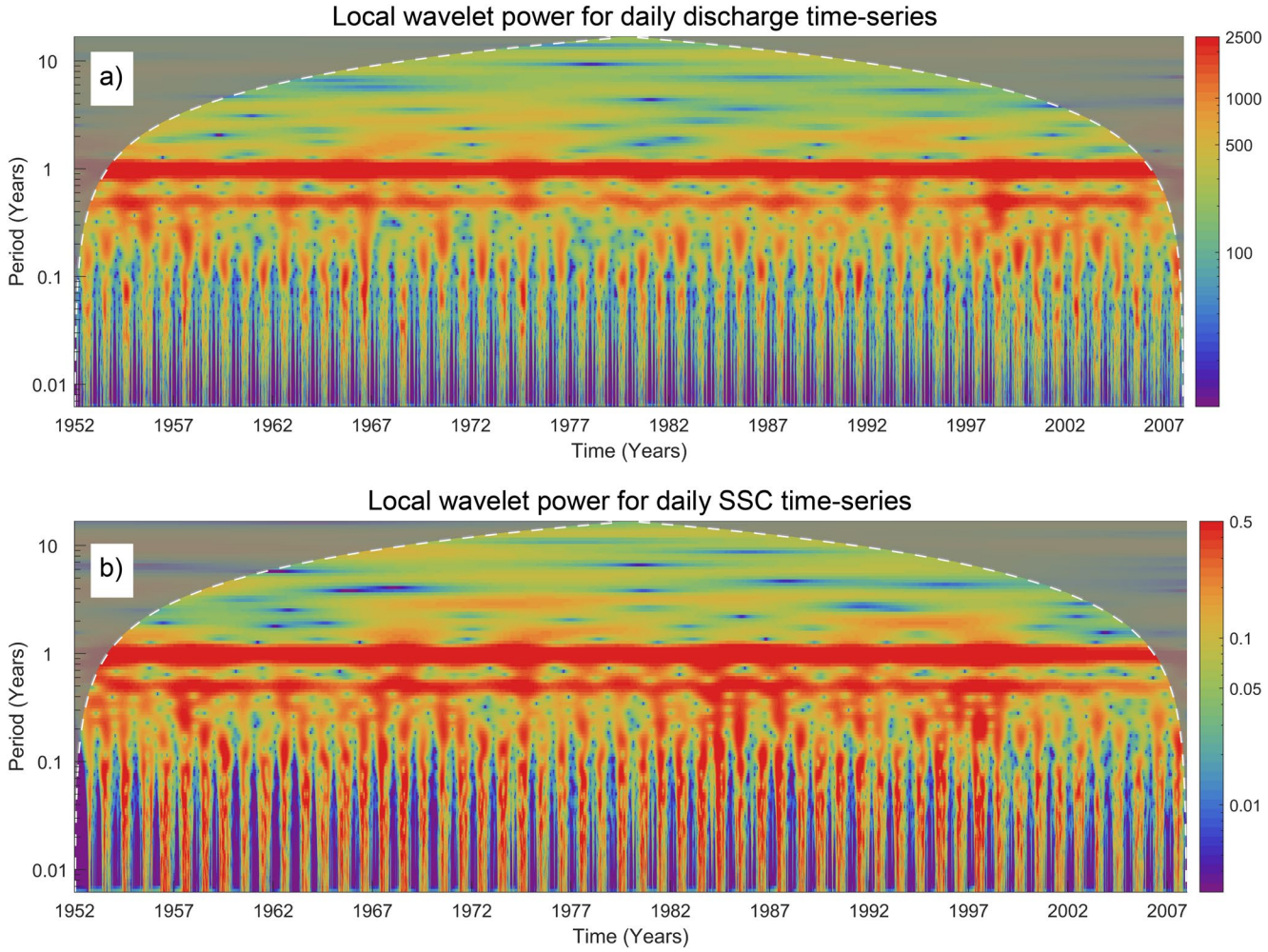

Figure 4. Local wavelet power spectrum of the daily discharge (a) and suspended sediment concentration (SSC) (b) time-series normalized by $1/STD^2$ (being STD the standard deviation). The vertical axis is the wavelet time-scale and the horizontal axis is the time position during the period 1957–2007 at Pingshan station. The shaded contours are at normalized variances of different local wavelet power. The thick white dashed curve depicts the cone of influence below which the edge effects on the amplitude of the local power spectrum are negligible (Torrence & Compo, 1998).

Table 1
Summary of the Temporal Variance Fraction Accounted by Each Dominant Time-Scale Determined Based on the Local and Global Power Spectra Displayed in Figures 2–4

	Temporal fraction	
Time-scale	Discharge	SSC
Intraseasonal-to-seasonal (<0.9 years)	0.34 (34%)	0.33 (33%)
Annual (0.9–1.1 yr)	0.40 (74%)	0.46 (79%)
Short-term-annual response (1.1–5.5 years)	0.18 (92%)	0.14 (93%)
Long-term-annual response (5.5–20 years)	0.08 (100%)	0.07 (100%)

Note. The variance fractions were obtained by applying the standard statistical variance formula to each wavelet time-series. Percentages in parentheses give incremental percentage of such temporal variance as the sum of the time-scales.
Abbreviation: SSC, suspended sediment concentration.

SSC records. Discharge seasonal variability is mainly clustered around a time-scale of 6 months (see Figure 2c), which identifies the hydrological cycle of the Upper Changjiang as a bi-modal cycle with high-flow (March–May and September–November) seasons and low-flow seasons (June–August and December–February) observed each year. These characteristics of the yearly discharge distribution reflect that Pingshan catchment follows a glacial-meltwater hydrological regime. The water flowing out the catchment is thus modulated by the freezing-thawing cycle of the Tibetan Plateau glaciers and winter snowpack and by intense precipitation for late summer and autumn. SSC yearly dynamics (see Figure 4) follow closely the discharge cycles. This indicates that most of the sediment is transported by the flow.

Short-term-annual and long-term time-scales for both discharge and SSC records account for 18%, 14%, 8%, and 7% of the total variability of each data set, respectively. Similar values are thus observed for discharge and SSC records, suggesting that the river is large and shows one major flood per year, which in principle control the yearly export of sediments.

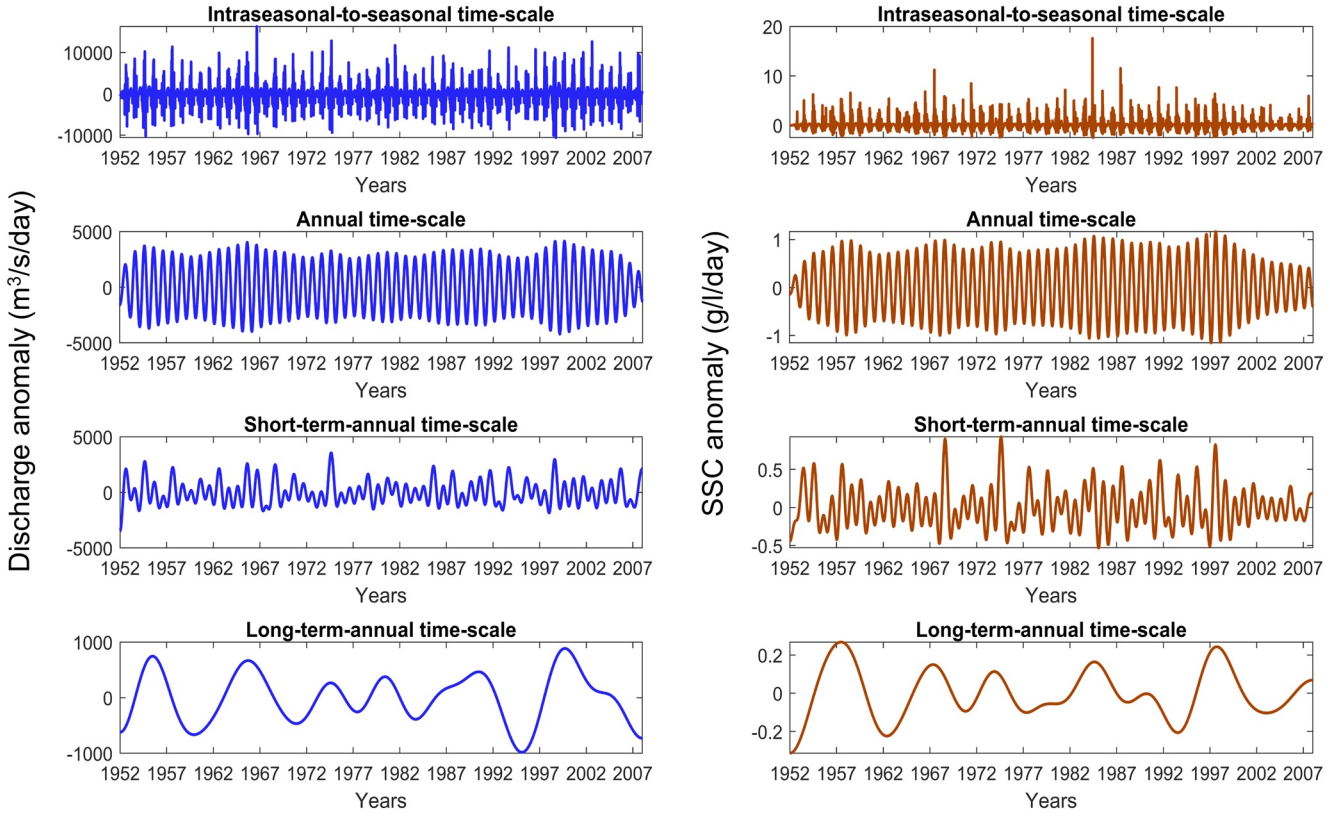

Figure 5. Temporal scale-by-scale de-composition of daily discharge time-series anomalies (left) and daily suspended sediment concentration (SSC) time-series anomalies (right). Positive and negative anomalies were calculated with respect to the mean values. The four non-overlapping time-scales bands contain the major power peaks and were determined based on the global power spectra displayed in Figures 2 and 4. Intraseasonal-to-seasonal time-scales represents a time band of 0.003–0.9 years; annual time-scale correspond to a time band of 0.9–1.1 years; short-term-annual time-scale depicts a time band of 1.1–5.5 years; long-term-annual time-scale is related with a time band of 5.5–20 years.

The intraseasonal-to-seasonal and annual time-scales displayed in Figure 5 show much more variable and larger anomalies values than short-term and long-term annual time-scales. Nonetheless, these anomalies vary rapidly (in short period of days) and thus, modulate repetitively the short-term (yearly) response of the Upper Changjiang. Discharge and SSC anomalies corresponding to the long-term-annual time-scale, despite being of smaller amplitudes, vary over a prolonged period and thus, modulate with positive or negative anomaly contributions the short-term response of the river-reach. Besides, intraseasonal-to-seasonal and short-term-annual time-scales, for both discharge and SSC records, possess larger positive anomalies than negative anomalies. Annual and long-term-annual time-scales have a balanced mix of positive and negative anomalies. Temporal trends throughout the period of analysis remain relatively constant for all the spectra of time-scales, except in the case of the SSC annual time-scale. From 1998, the annual signal exhibits a significant decay. This is reflected in the discharge annual anomaly where the decay values from 1998 display a continuous decay with regard to the previous period.

4.2. Sediment Fluxes Dynamics at Pingshan Station

Temporal variations in suspended sediment fluxes for the overall SSC records and for each dominant time-scale identified in Figures 2–4 are presented in Figure 6. This analysis reveals that the intra-seasonal and annual time-scales possess a positive value throughout the period of analysis (i.e., a sustained sediment inflow). On the contrary, the multi-annual time-scales (see Figures 6d and 6e) display an alternating cycle of positive and negative values of sediment fluxes (i.e., an excess or deficit of sediment fluxes with respect to the mean).

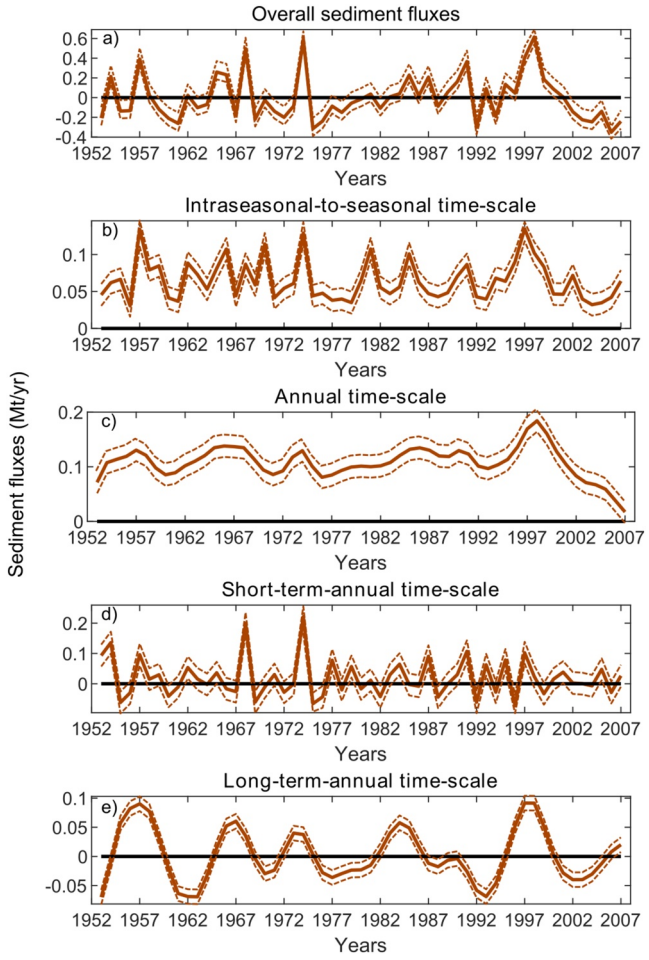

Figure 6. (a) Overall variation of yearly sediment fluxes for the period 1952–2007 at Pingshan station. Temporal scale-by-scale decomposition of yearly sediment fluxes; (b) at intraseasonal-to-seasonal time-scale; (c) at annual time-scale; (d) at short-term-annual time-scale; (e) at long-term-annual time-scale. Results were computed by estimating the sediment fluxes on the basis of daily discharge and suspended sediment concentration values, and summed to determine the yearly results. Furthermore, results were normalized by subtracting the mean value for the 1952–2007 period. A significant drop in the supply of suspended sediments at annual time-scale from 1998 until the end of our study period is noted. Dashed lines represent the estimated error range for each year, ±10%.

The cumulative sediment departure plot identifies years with increasing and decreasing sediment fluxes trends (see Figure 7). Accordingly, sustained increasing and decreasing patterns of cumulative sediment departure values correspond to excess or deficit of sediment fluxes with respect to previous years.

4.3. Coupling Between Discharge and SSC Records

In this section, we explore the coupling between the discharge and SSC time-series. We use: (a) a traditional magnitude-frequency analysis to infer estimates of the discrete probability density function of discharge and SSC values based on the ensemble data, and (b) a more sophisticated wavelet coherence analysis, which compares the two wavelet spectra, thus identifying the episodic transient patterns which oscillates at a similar time-scale and for the same time period.

Discrete magnitude frequency curves are similar for both discharge and SSC time-series (see Figure 8). It is noted that even for low discharges, SSC values are recorded, which reflects the continuous suspended sediment supply. The date of event of the largest floods and SSC observations do not coincide, which indicates that flow alone is not the only driver of the sediment dynamics.

The squared wavelet coherence (see Figure 9) between discharge and SSC time-series display weak wavelet coherence for time-scales below 0.5 years. This is not surprising since time-shifts for discharge-SSC relations are influenced by precipitation intensity and areal distribution, runoff amount and rate, floodwater travel rates and travel distances, spatial and temporal storage-mobilization-depletion processes of available sediment, and sediment travel rates and distances. Given the large catchment area, the potential mix and interrelations of these and other variables limit the possibility of clearly identify the time-shifts for short time-scales. On the other hand, strong coupling occurs at the seasonal (around 0.5 years) and annual time-scale due to the high synchronicity in the annual dynamics of discharge and resulting sediment transport (see the strong similarity of the global power spectra in Figures 2 and 3). Right arrows in these time-scales indicate no significant delay between discharge and SSC time-series all throughout the study period. At larger time-scales (5–16 years) is interesting to note a strong wavelet coherence but with changing dynamics. During 1957 to 1977, the arrows point vertically upward, which indicate discharge peaks before SSC, that is, a counter-clockwise sediment hysteresis loop. On the contrary, for the period of 1985–2000, the arrows point down, thus indicating SSC peaks before discharge.

5. Discussion

5.1. Temporal Description of the Catchment and River Processes Governing the Sediment Budget Dynamics of the Upper Changjiang at Pingshan Station

The analysis of long-term data sets of measured discharge and SSC in large river networks integrates a wide range of processes acting at different time and spatial scales. We interpret such processes, which ultimately drive the long-term sediment dynamics at Pingshan station.

Examination of the temporal structure of the discharge and SSC time-series at Pingshan station reveals four dominant time-scales accounting for intraseasonal-to-seasonal, annual; short-term-annual and

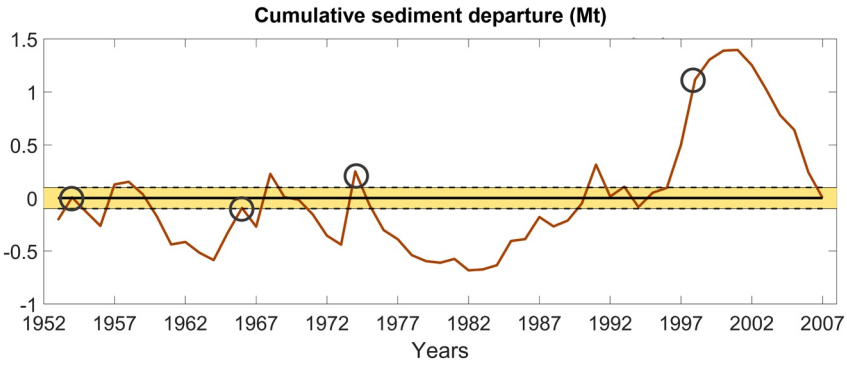

Figure 7. Variation of cumulative sediment departure for the period 1952–2007 at Pingshan station. Results were normalized by subtracting the mean value for the study period. Decreasing sediment departure trends are observed in 1960–1964, 1974–1982, and in 2002–2007. Notable increasing sediment departure trends are observed in 1965–1970, 1983–1993, and in 1997–2000. Periods without a clear trend are found in 1957–1960 and in 1993–1995. Shaded areas represent the estimated error range reffering to the mean, ±10%. Location of the four largest floods identified in Figure 8 are shown by circles.

long-term-annual time-scales (see Table 1). The short time-scales (≤1 year) are mainly modulated by the seasonal climatological patterns typical of a glacial-meltwater hydrological regime with a bi-modal seasonal pattern: dominant time-scale of 6 months, see Figures 2 and 3 (Déry et al., 2009; Konovalov & Rudakov, 2018). High-flow values are recorded twice a year: during the snowmelt season (March–April: this is the dominant annual flow peak identified in Figure 2b) and during late summer and autumn (September–November: this is the second major high flow peak of the year identified in Figure 2c). This latter high-flow events period is related with the annual precipitation distribution of the Tibetan Plateau Mountains, from which most of the water recorded at Pingshan comes from. Precipitation rates during the months of June–October are high (Wan et al., 2017). However, the high temperatures and related high evapotranspiration processes prevent surface runoff, and thereby the occurrence of floods during most of the summer. Accordingly, only in late summer and autumn, with the drop of temperatures, high-flow values are observed.

Furthermore, most of the temporal variability, for both the discharge and SSC time-series, is accounted by the short time-scales (intraseasonal and annual time-scales, see Table 1). This implies that discharge, driven by seasonal patterns (i.e., intra-annual periods of high and low flow discharge), is the major control of sediment supply and resulting SSC observations (Millares et al., 2020; Vercruysse et al., 2017). Looking at the contribution of such short time-scales to the sediment dynamics, a positive trend above the overall mean records is consistently computed (see Figures 6b and 6c). Sediment supplied by short time-scales thus tend to be large sediment contributors relative to the long-term time-scales mean. This is not surprising since as noted by Hassan et al. (2011) around 75% of the sediment comes from upstream Pingshan station, mainly

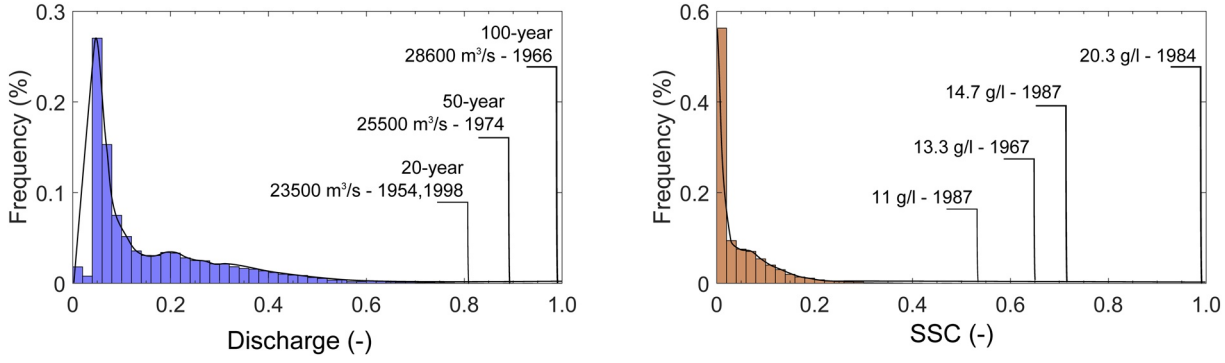

Figure 8. Discrete probability density function of the discharge (left) and suspended sediment concentration (SSC) (right) time-series during the period 1952–2007 at the gauging station of Pingshan. Results were normalized by the maximum of each time-series. The four largest values are identified and the magnitude, date of event, and corresponding return period (for the discharge) are provided.

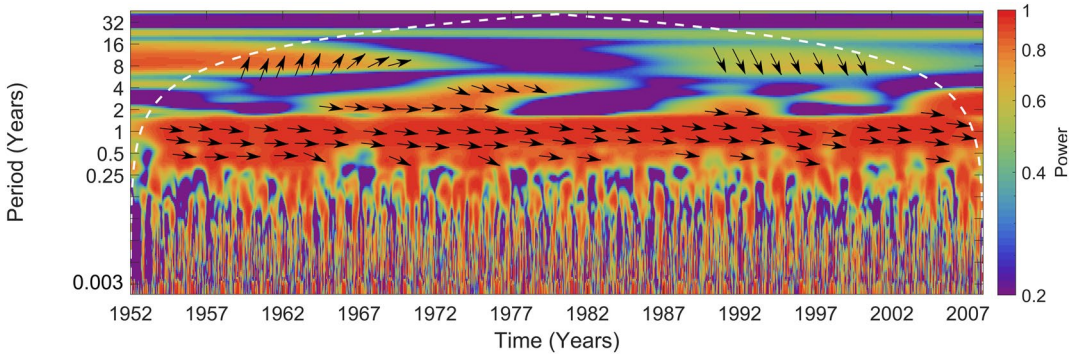

Figure 9. Squared wavelet coherence between discharge and suspended sediment concentration (SSC) time-series during the period 1952–2007 at the gauging station of Pingshan. The vertical axis is the time-scale and the horizontal line is the time position. The dashed curve depicts the cone of influence within which the edge effects are negligible. The shaded contours indicate the strength of the coherence. Arrows are plotted for time-scales above 0.5 years and in those regions where coherence is significant above the 60% level. Directions of the arrows indicate the degree to which discharge and SSC time-series are in phase or have a time delay, that is, the arrows serve to identify the coupling between the two signals. Right arrows indicate discharge and SSC time-series are in phase (0°), left arrows indicate discharge and SSC time-series are completely out of phase (180°). An arrow pointing vertically upward (90°) means SSC lags discharge by one fourth of the cycle at that time-scale. An arrow pointing vertically downwards (phase angle of −90° or 270°) means SSC peaks before discharge by one fourth of the cycle at that time-scale.

from the Tibetan Plateau Mountains, where sediment sources are abundant. This sediment supply from the mountains is delivered by the mainstem, by either small or large tributaries and episodically by landslides and debris flow triggered at the headwaters. The remaining 25% of the sediment recorded at Pingshan is contributed by other sediment sources from the landscape. Furthermore, the river is confined and incised into bedrock, forming a deep canyon. Consequently, sediment transport losses due to floodplains sedimentation are negligible. The resulting dominant contribution of the sediment delivered by the upstream mainstem of Pingshan and the existence of steep slopes (which provide the flow with energy enough to convey rapidly the sediments produced at the headwaters) lead to a strong synchronicity between discharge and SSC at seasonal and annual scales (see Figure 9). The suspended sediment fluxes are clearly correlated with the occurrence of high flood events in late summer and autumn and to the snowmelt period (dominant time-scale of 6 months, see Figures 2 and 3), indicating that these are the two most intense periods of hydrological and geomorphic activity in the catchment at intra-annual time-scales.

Large time-scales (>1 year) identified in the temporal spectrum of the discharge and SSC time-series are mainly related to large magnitude flow events which have enough flow capacity to supply more sediments and/or to re-mobilize in-channel stored sediments. These time-scales just explained 26% and 21% of the temporal variability for the discharge and SSC time-series, respectively (see Table 1). However, the role of these inter-annual time-scales is of particular interest because their contribution to the sediment fluxes fluctuates between transient periods of positive and negative values (see Figures 6d and 6e). For a clearer discussion, we split the large time-scales into short-term-annual (1.1–5.5 years) and long-term annual time scales (5.5–20 years) as already displayed in Table 1.

Comparing the cumulative sediment departures in Figure 7 and the largest flooding events identified in Figure 8-left, which belong to the long-term-annual time-scales, we observe that the largest flooding events are related consistently with an increase of the cumulated values of sediment loads (D. Li, Li, et al., 2020; Z. Li, Xu, et al., 2020). However, the largest observations of SSC (see Figure 8-right) were not recorded the same year as the largest floods occurred (Gonzalez-Hidalgo et al., 2013). Consequently, we conclude that the largest floods are likely to mobilize large amounts of sediment, and a part of this material is accumulated in the channel (Gonzalez-Hidalgo et al., 2010). The long-term time-scales related to the largest floods thus dictate in the long-term the increasing or decreasing cumulative sediment departure temporal trends.

Conversely, all inflections in the cumulative sediment departures showed in Figure 7 correspond to moderate floods, which are related to short-term-annual time-scales. This indicates that short-term-annual related floods are primary proxies of the channel changes but alone do not control the final outcome.

An additional interesting point about the short-term-annual time-scales is that, although most of the SSC temporal fluctuations are first triggered by discharge fluctuations, there are some years with abnormal large SSC peaks anomalies, which are not correlated with large discharge anomalies neither at short nor at long-term-annual time-scales (see Figure 5). For instance, we noted large SSC anomaly peaks within the short-term-annual spectrum in 1954, 1968, or 1977 and not concurrent similar large discharge anomalies were recorded those years. That punctual and transient increase in the sediment records cannot be related to discharge (and by implication with in-channel sediments). Instead, we suggest they are owed to relatively large sediment inputs from the landscape probably originated in the upper catchment (Hassan et al., 2011). Field evidence indicates that occasional mass movement activity occurs in the steep terrain upstream of Pingshan station (Cai, 1998; Z. Y. Wang et al., 2007; Xu, 2009). This massive sediment delivery to the river by means of landslides thus leaves its signature in the short-term-annual time-scale.

The computation of the cumulative sediment departures displays a varying succession of increasing and decreasing trends observed all throughout the years (see Figure 7). However, in the long term, the cumulative variation of positive and negative departures from the mean is quasi-steady and it keeps the river reach within equilibrium (close to the mean) or little increasing trend. This highlights the importance of using a long-term data set to infer accurate and reliable estimates of the functioning of the fluvial system.

Results from wavelet coherence analysis in Figure 9 reveal that sediment residence time at Pingshan station is low. The discharge and SSC time-series are highly synchronized at intra-annual and annual scales (sediment inputs and outputs within-reach are similar). Only for 1957–1977 discharge signal peaks before SSC (i.e., a counter-clockwise sediment hysteresis), which, according to several authors such as Phillips et al. (1999) or Juez et al. (2018), implies that sediment source is not exhausted and part of the supplied sediments is not evacuated from the river reach. We obtained a resulting sediment resident time between 5 and 16 years (see the strong wavelet coherence at time-scales 5 to 16 in Figure 9). This time is intrinsically site-specific, only valid for Pingshan station and it is controlled by the confinement and other characteristics of the catchment (Jantzi et al., 2017).

The transient patterns determined from the discharge and SSC temporal spectrum are not static all throughout the study period and a main temporal shift was identified and related to land use changes. In the early-mid 1970s China launched a national soil conservation program. These measures brought under control large areas of the Changjiang landscapes, which formerly were eroding rapidly, resulting in a major decline in sediment mobilization from the basin (Hassan et al., 2010). Looking at the variation of the cumulative sediment departures in Figure 7, we observe that since 1982 the decreasing cumulative sediment departure trend was reversed without the occurrence of a major flood. In 1998, due to the major flood (the fourth largest one observed in the study period) the increasing trend was notably increased, although the channel quickly migrated toward balance, reached in 2007. This change in the temporal trends is further supported by the shift in the coupling between discharge and SSC identified in Figure 9 at the long-term-annual time-scales (time-scales between 5 and 16 years). For 1957–1977 discharge signal peaks before SSC, but for 1985–2000 the tendency is reversed and SSC peaks before. According to several authors (e.g., Andermann et al., 2012; Juez et al., 2018; Walling et al., 1998), a delayed SSC peak with respect to discharge peak corresponds to accumulation of in-channel sediments. We thus believe that this markedly change in the coupling between discharge and SSC was owned by the implementation of the soil conservation measures. We can thus affirm that the temporal gap with asynchrony between discharge and SSC (1977–1985, see Figure 9) is related with the time-frame required by the soil protection measures to took a full effect on the sediment dynamics of the Upper Changjiang.

5.2. Differences of Wavelet Analysis Regarding Deterministic and Machine-Learning Models

The application of the wavelet analysis to our high variable time-series proves useful to understand the underlying processes governing the sediment production and transport processes in a large catchment. This technique overcomes difficulties faced by other deterministic or machine-learning techniques, which also endeavors to understand such catchment/river processes. In the case of deterministic techniques, based on physical laws, there is a need for a detailed spatial description of the catchment characteristics (grain size, flow depth and velocity, channel slope, land use, and land cover, etc.) as a basis for obtaining accurate results. However, this detailed spatial description is a snapshot of the catchment conditions taken at a

fixed time. Thereby, it does not include the previous history of the catchment and the contribution of large time-scales.

Relating to machine-learning techniques, we overcome such physical constraint thanks to its data-driven nature. In this case, the model is trained by subsets of data (representatives of the whole data set) and it is capable of fitting the rest of the data set. However, the physical processes governing the data sets dynamics cannot be directly inferred from the results. In turn, they can be surmised and assessed. For instance, in Matos et al. (2018), the influence of seasonal and local contributions to SSC concentrations recorded at Pingshan station was assessed by conditioning the probability estimation on seasonal and local drivers. This pre-conditioning process requires a prior knowledge/intuition of the catchment dynamics. Furthermore, machine learning basis relies on the statistical stationary time-series, which implies that episodic large/low magnitude events (owing to the large time-scales) are not well modeled and consequently, understood.

In contrast, the wavelet analysis disentangled the long-term time-series, thus allowing to learn from their temporal structure. We perform a photo sequence analysis rather than a fixed photo analysis (deterministic techniques) of the catchment and river conditions. Furthermore, we time-localized the governing processes and their variability at any time of the study period (contrary to classic Fourier spectral analysis and entropy analysis), rather than estimate and assess the ensemble dominant process within the whole data set (contrary to machine-learning techniques). The continuous variability of each time-scale is thus identified and quantified in a valuable way (see Figure 6).

6. Conclusions

The temporal structure of the concurrent discharge and SSC time-series recorded at Pingshan station, at the Upper Changjiang, was herein analyzed by means of the wavelet analysis. The long-term data set allows to explore the nature of episodic transient patterns of water and sediment fluxes and relate them to catchment and river processes occurring at different and non-similar time-scales.

The results illustrate that at Pingshan station four time-scales accounting for intraseasonal-to-seasonal, annual, short-term-annual and long-term-annual time-scales control the temporal variability of the discharge and SSC data. The short time-scales (<1 year) are driven by the climatic characteristics of the uppermost region of the catchment (i.e., the Tibetan Plateau glaciers) and they account themselves for most of the temporal variability in both the discharge and SSC time-series. These results indicate that discharge is the major driver of the sediment fluxes on yearly basis. Furthermore, these short time-scales provide a continuous sediment supply, which translates into positive sediment contribution to the total sediment budget of the river reach.

On the other hand, the large time-scales (>1 year) despite of contributing to less than 26% to the total temporal variability of the time-series, play a major role on the river reach dynamics. They are driven by: (a) events of high magnitude (low frequency) which have larger flow capacity to transport and/or to re-mobilize in-channel stored sediments deposited by the intraseasonal-to-seasonal, annual or inter-annual time-scales, and (b) mass movements, which deliver punctual sediment loads to the river. The contribution of these larger time-scales to the sediment fluxes fluctuates between transient periods of positive and negative values. We prove that flow alone is not the only driver of the sediment dynamics and in-channel sediments ultimately controls the resulting positive or negative balance. We thus show that a correct sediment analysis cannot solely rely on annual estimates of sediment fluxes. The inter-annual time-scales and possible land uses changes play a major control of the sediment dynamics and ultimately of the river channel changes.

Finally, the skillful analysis of the temporal structure of the data set provided by the wavelet transform method handles the long-term data set (contrary to pure deterministic methods) and non-stationary time-series (contrary to machine learning methods). Thus, it can be of great help for river networks and catchment management since it can detect and identify any land use change or climate shift, which eventually drive to different water and sediment fluxes. This information improves the understanding of the mechanics underlying the within-sediment reach balance and has important societal relevance for activities such as flood forecasting, reservoir operation or afforestation practices.

Data Availability Statement

The base data of the paper can be found at: https://saco.csic.es/index.php/s/GoyLWmMm8sbS8bi. Further instructions on how to access and use the base data can be found in the supporting information.

Acknowledgments
This work was funded by the H2020-MSCA-IF-2018 programme (Marie Sklodowska-Curie Actions) of the European Union under REA grant agreement, number SEDILAND-834329. The authors are grateful to the Changjiang Commission of Water Resources for access to the hydrological data. Spatial thanks are extended to Dr. Chenge An from the Tsinghua University and Lily Liu from the University of British Columbia for helping in the translation of texts from Chinese to English. Thanks are also due to the six reviewers and the Associate Editor, whose insightful, thoughtful, and helpful comments greatly improved the quality of the final paper.

References

Andermann, C., Crave, A., Gloaguen, R., Davy, P., & Bonnet, S. (2012). Connecting source and transport: Suspended sediments in the Nepal Himalayas. *Earth and Planetary Science Letters*, *351*, 158–170. https://doi.org/10.1016/j.epsl.2012.06.059

Ashworth, P., & Ferguson, R. (1986). Interrelationships of channel processes, changes and sediments in a proglacial braided river. *Geografiska Annaler Series A, Physical Geography*, *68*(4), 361–371. https://doi.org/10.2307/521527

Asselman, N. E. M. (2000). Fitting and interpretation of sediment rating curves. *Journal of Hydrology*, *234*, 228–248. https://doi.org/10.1016/S0022-1694(00)00253-5

Baxter, C., & Hauer, F. (2000). Hyporheic exchange, and selection of spawning habitat by bull trout (Salvelinus Confluentus). *Canadian Journal of Fisheries and Aquatic Sciences*, *57*, 1470–1481. https://doi.org/10.1139/cjfas-57-7-147010.1139/f00-056

Boix-Fayos, C., Nadeu, E., Quiñonero, J., Martínez-Mena, M., Almagro, M., & de Vente, J. (2015). Sediment flow paths and associated organic carbon dynamics across a Mediterranean catchment. *Hydrological Earth System Sciences*, *19*(3), 1209–1223. https://doi.org/10.5194/hess-19-1209-2015

Cai, Z. X. (1998). Building the flood-protection system in Schaun province: The role of soil conservation. *Soil Conservation Changjiang Basin*, *4*, 20–22.

Carey, S. K., Tetzlaff, D., Buttle, J., Laudon, H., McDonnell, J., McGuire, K., et al. (2013). Use of color maps and wavelet coherence to discern seasonal and interannual climate influences on streamflow variability in northern catchments. *Water Resources Research*, *49*, 6194–6207. https://doi.org/10.1002/wrcr.20469

Chen, J., Wu, X., Finlayson, B., Webber, M., Wei, T., Maotian, L., & Chen, Z. (2014). Variability and trend in the hydrology of the Yangtze River, China: Annual precipitation and runoff. *Journal of Hydrology*, *513*, 403–412. https://doi.org/10.1016/j.jhydrol.2014.03.044

Chen, X. Q., Yan, Y., Fu, R. S., Dou, X., & Zhang, E. F. (2008). Sediment transport from the Changjiang, China, into the sea over the Post-Three Gorge Dam Period: A discussion. *Quaternary International*, *186*, 55–64. https://doi.org/10.1016/j.quaint.2007.10.003

Chen, Z., Li, J. F., Shen, H. T., & Wang, Z. H. (2001). Yangtze River of China: Historical analysis of discharge variability and sediment flux. *Geomorphology*, *41*, 377–391. https://doi.org/10.1016/S0169-555X(01)00106-4

Chen, Z., Yu, L., & Gupta, A. (2001). The Yangtze River: An introduction. *Geomorphology*, *41*, 373–375. https://doi.org/10.1016/S0169-555X(01)00105-2

Chien, N., & Wan, Z. (1999). *Mechanics of sediment transport*. American Society of Civil Engineers, ASCE Press.

Choubin, B., Darabi, H., Rahmati, O., Sajedi-Hosseini, F., & Kløve, B. (2018). River suspended sediment modelling using the CART model: A comparative study of machine learning techniques. *Science of the Total Environnent*, *615*, 272–281. https://doi.org/10.1016/j.scitotenv.2017.09.293

Cox, L. (2008). What's wrong with risk matrices? *Risk Analysis*, *28*(2). https://doi.org/10.1111/j.1539-6924.2008.01030.x

Déry, S. J., Stahl, K., Moore, R. D., Whitfield, P. H., Menounos, B., & Burford, J. E. (2009). Detection of runoff timing changes in pluvial, nival, and glacial rivers of western Canada. *Water Resources Research*, *45*, W04426. https://doi.org/10.1029/2008WR006975

De Vries, A., & Klavers, H. C. (1994). Riverine fluxes of pollutants: Monitoring strategy first, calculation methods second. *European Water Pollution Control*, *4*, 12–17. https://doi.org/10.1016/j.crte.2007.05.001

Gao, P. (2008). Understanding watershed suspended sediment transport. *Progress in Physical Geography: Earth and Environment*, *32*(3), 243–263. https://doi.org/10.1177/0309133308094849

Gao, P., Nearing, M. A., & Commons, M. (2013). Suspended sediment transport at the instantaneous and event time scales in semi-arid watersheds of southern Arizona, USA. *Water Resources Research*, *49*, 1–14. https://doi.org/10.1002/wrcr.20549

Gonzalez-Hidalgo, J. C., Batalla, R. J., & Cerda, A. (2013). Catchment size and contribution of the largest daily events to suspended sediment load on a continental scale. *Catena*, *102*, 40–45. https://doi.org/10.1016/j.catena.2010.10.011

Gonzalez-Hidalgo, J. C., Batalla, R. J., Cerdà, A., & de Luis, M. (2010). Contribution of the largest events to suspended sediment transport across the USA. *Land Degradation & Development*, *21*, 83–91. https://doi.org/10.1002/ldr.897

Grinsted, A., Moore, J. C., & Jevrejeva, S. (2004). Application of the cross wavelet transform and wavelet coherence to geophysical time series. *Nonlinear Processes in Geophysics*, *11*, 561–566. https://doi.org/10.5194/npg-11-561-2004

Hassan, M. A., Church, M., Yan, Y., & Slaymaker, O. (2010). Spatial and temporal variation of in-reach suspended sediment dynamics along the mainstem of Changjiang (Yangtze River), China. *Water Resources Research*, *46*, W11551. https://doi.org/10.1029/2010WR009228

Hassan, M. A., Church, M., Yan, Y., Slaymaker, O., & Xu, J. (2011). Suspended sediment balance for the mainstem of Changjiang (Yangtze River) in the period 1964-1985. *Hydrological Processes*, *25*, 2339–2353. https://doi.org/10.1002/hyp.7996

Higgitt, D. L., & Lu, X. X. (1999). Challenges in relating land use to sediment yield in the Upper Yangtze, China. *Hydrobiologia*, *410*, 269–277. https://doi.org/10.1023/A:1003850418543

Horowitz, A. J. (1995). *The use of suspended sediment and associated trace elements in water quality studies* (IAHS Special Publication No. 4, p. 58). IAHS Press.

Horowitz, A. J. (2003). An evaluation of sediment rating curves for estimating suspended sediment concentrations for subsequent flux calculations. *Hydrological Processes*, *17*, 3387–3409. https://doi.org/10.1002/hyp.1299

Horowitz, A. J., Elrick, K. A., & Smith, J. J. (2001). Estimating suspended sediment and trace element fluxes in large river basins: Methodological considerations as applied to the NASQAN program. *Hydrological Processes*, *15*, 1107–1132. https://doi.org/10.1002/hyp.206

Jantzi, H., Liébault, F., & Klotz, S. (2017). Sediment residence time in alluvial storage of black marl badlands. *Catena*, *156*, 82–91. https://doi.org/10.1016/j.catena.2017.03.026

Juez, C., Hassan, M. A., & Franca, M. J. (2018). The origin of fine sediment determines the observations of suspended sediment fluxes under unsteady flow conditions. *Water Resources Research*, *48*, 5654–5669. https://doi.org/10.1029/2018WR022982

Juez, C., & Nadal-Romero, E. (2020a). Long-term temporal structure of catchment sediment response to precipitation in a humid mountain badland area. *Journal of Hydrology*, *191*, 125723. https://doi.org/10.1016/j.jhydrol.2020.125723

Juez, C., & Nadal-Romero, E. (2020b). Long-term time-scale bonds between discharge regime and catchment specific landscape traits in the Spanish Pyrenees. *Environmental Research*, *191*, 110–158. https://doi.org/10.1016/j.envres.2020.110158

Juez, C., Schärer, C., Jenny, H., Schleiss, A. J., & Franca, M. J. (2019). Floodplain land cover and flow hydrodynamic control of overbank sedimentation in compound channel flows. *Water Resources Research*, *55*, 9072–9091. https://doi.org/10.1029/2019WR024989

Konovalov, V., & Rudakov, V. (2018). Hydrological regime of glaciers in the river basins of the Northern Caucasus and Altai. *Ice and Snow*, *58*, 21–40. https://doi.org/10.15356/2076-6734-2018-1-21-40

Kumar, D., Pandey, A., Sharma, N., & Flügel, W. A. (2015). Daily suspended sediment simulation using machine learning approach. *Catena*, *138*, 77–90. https://doi.org/10.1016/j.catena.2015.11.013

Labat, D., Ronchail, J., & Guyot, J. L. (2005). Recent advances in wavelet analyses: Part 2: Amazon, Parana, Orinoco and Congo discharges time scale variability. *Journal of Hydrology*, *314*, 289–311. https://doi.org/10.1016/j.jhydrol.2005.04.004

Lamb, M. P., de Leeuw, J., Fischer, W. W., Moodie, A. J., Venditti, J. G., Nittrouer, J. A., et al. (2020). Mud in rivers transported as flocculated and suspended bed material. *Nature Geoscience*, *13*(8), 566–570. https://doi.org/10.1038/s41561-020-0602-5

Li, D., Li, Z., Zhou, Y., & Lu, X. (2020). Substantial increases in the water and sediment fluxes in the headwater region of the Tibetan Plateau in response to global warming. *Geophysical Research Letters*, *47*, e2020GL087745. https://doi.org/10.1029/2020GL087745

Li, J., Xie, S., & Kuang, M. (2001). Geomorphic evolution of the Yangtze Gorges and the time of their formation. *Geomorphology*, *41*, 125–135. https://doi.org/10.1016/S0169-555X(01)00110-6

Li, Z., Xu, X., Zhu, J., Xu, C., & Wang, K. (2020). The contributions of the largest erosive events to sediment yields in karst catchments. *Water Resources Research*, *56*. https://doi.org/10.1029/2019WR025839

Lu, X. X., & Higgitt, D. L. (1998). Recent changes of sediment yield in the Upper Yangtze, China. *Environmental Management*, *22*, 697–709. https://doi.org/10.1007/s002679900140

Lu, X. X., & Higgitt, D. L. (1999). Sediment yields variability in the Upper Yangtze. *Earth Surface Processes and Landforms*, *24*, 1077–1093. https://doi.org/10.1002/(SICI)1096-9837(199911)24:12<1077::AID-ESP36>3.0.CO;2-M

Matos, J. P., Hassan, M. H., Xixi, L., & Franca, M. J. (2018). Probabilistic prediction and forecast of daily suspended sediment concentration on the upper Yangtze River. *Journal of Geophysical Research: Earth Surface*, *124*, 1982–2003. https://doi.org/10.1002/2017JF00424010.1029/2017jf004240

McLean, D. G., Church, M., & Tassone, B. (1999). Sediment transport along lower Fraser River. 1. Measurements and hydraulic computations. *Water Resources Research*, *35*(8), 2533–2548. https://doi.org/10.1029/1999WR900101

Millares, A., Chikh, H. A., Habi, M., Morsli, B., Galve, J. P., Perez-Peña, J. V., & Martín-Rosales, W. (2020). Seasonal patterns of suspended sediment load and erosion-transport assessment in a Mediterranean basin. *Hydrological Sciences Journal*, *65*(6), 969–983. https://doi.org/10.1080/02626667.2020.1724294

Ministry of Water Resources of the People's Republic of China. (1952–2007). *Annual hydrological report, People's Republic of China: Hydrological data of Changjiang river basin*.

Patil, S., Sivapalan, M., Hassan, M. A., Ye, S., Harman, C. J., & Xu, X. (2012). A network model for prediction and diagnosis of sediment dynamics at the watershed scale. *Journal of Geophysical Research*, *117*, F00A04. https://doi.org/10.1029/2012JF002400

Phillips, J. M., Webb, B. W., Walling, D. E., & Leeks, G. J. L. (1999). Estimating the suspended sediment loads of rivers in the LOIS study area using infrequent samples. *Hydrological Processes*, *13*, 1035–1050. https://doi.org/10.1002/(SICI)1099-1085(199905)13:7<1035::AID-HYP788>3.0.CO;2-K

Regüés, D., & Nadal-Romero, E. (2013). Uncertainty in the evaluation of sediment yield from badland areas: Suspended sediment transport estimated in the Araguás catchment (central Spanish Pyrenees). *Catena*, *106*, 93–100. https://doi.org/10.1016/j.catena.2012.05.006

Rhoads, B. L. (2020). *River dynamics: Geomorphology to support management*. Cambridge University Press.

Rijn, L. C. V. (1984). Sediment transport, part II: Suspended load transport. *Journal of Hydraulic Engineering*, *110*(11), 1613–1641. https://doi.org/10.1061/(asce)0733-9429(1984)110:11(1613)

Salant, N. L., Hassan, M. A., & Alonso, C. V. (2008). Suspended sediment dynamics at high and low storm flows in two small watersheds. *Hydrological Processes*, *22*, 1573–1587. https://doi.org/10.1002/hyp.6743

Santini, W., Camenen, B., Le Coz, J., Vauchel, P., Guyot, J.-L., Lavado, W., et al. (2019). An index concentration method for suspended load monitoring in large rivers of the Amazonian foreland. *Earth Surface Dynamics*, *7*(2), 515–536. https://doi.org/10.5194/esurf-2018-9310.5194/esurf-7-515-2019

Schleiss, A. J., Franca, M. J., Juez, C., & De Cesare, G. (2016). Reservoir sedimentation. *Journal of Hydraulic Research*, *54*(6), 595–614. https://doi.org/10.1080/00221686.2016.1225320

Segele, Z., Lamb, P., & Leslie, L. (2009). Seasonal-to-interannual variability of Ethiopia/Horn of Africa monsoon. Part I: Associations of wavelet-filtered large-scale atmospheric circulation and global sea surface temperature. *Journal of Climate*, *22*, 3396–3421. https://doi.org/10.1175/2008JCLI2859.1

Smith, B. P. G., Naden, P. S., Leeks, G. J. L., & Wass, P. D. (2003a). Characterizing the fine sediment budget of the River Swale, Yorkshire, UK during the 1994 to 1995 winter season. *Hydrobiology*, *494*, 135–143. https://doi.org/10.1023/A:1025401929089

Smith, B. P. G., Naden, P. S., Leeks, G. J. L., & Wass, P. D. (2003b). The influence of storm events on fine sediment transport, erosion and deposition within the River Swale, Yorkshire, UK. *Science of the Total Environment*, *314*, 451–474. https://doi.org/10.1016/s0048-9697(03)00068-8

Smith, L. C., Turcotte, D. L., & Isacks, B. L. (1998). Stream flow characterization and feature detection using a discrete wavelet transform. *Hydrological Processes*, *12*, 233–249. https://doi.org/10.1002/(SICI)1099-1085(199802)12:2<233::AID-HYP573>3.0.CO;2-3

Smith, S. M. C., Belmont, P., & Wilcock, P. R. (2013). Closing the gap between watershed modeling, sediment budgeting, and stream restoration. In A. Simon, S. J. Bennet, & J. M. Castro (Eds.), *Stream restoration in dynamic fluvial systems: Scientific approaches, analyses, and tools* (pp. 293–317). American Geophysical Union. https://doi.org/10.1029/2011gm001085

Sternecker, K., Wild, R., & Geist, J. (2013). Effects of substratum restoration on salmonid habitat quality in a subalpine stream. *Environmental Biology of Fishes*, *22*, 376–396. https://doi.org/10.1007/s10641-013-0111-0

Torrence, C., & Compo, G. P. (1998). A practical guide to wavelet analysis. *Bulletin of the American Meteorological Society*, *79*, 61–78. https://doi.org/10.1175/1520-0477(1998)07910.1175/1520-0477(1998)079<0061:apgtwa>2.0.co;2

Tsuruta, K., Hassan, M. A., Donner, S. D., & Alila, Y. (2018). Development and application of a large-scale, physically based, distributed suspended sediment transport model on the Fraser River Basin, British Columbia, Canada. *Journal of Geophysical Research: Earth Surface*, *123*, 2481–2508. https://doi.org/10.1029/2017JF004578

Vercruysse, K., Grabowski, R. C., & Rickson, R. J. (2017). Suspended sediment transport dynamics in rivers: Multi-scale drivers of temporal variation. *Earth-Science Reviews*, *166*, 38–52. https://doi.org/10.1016/j.earscirev.2016.12.016

Walling, D. E. (1977). Assessing the accuracy of suspended sediment rating curves for a small basin. *Water Resources Research*, *13*, 531–538. https://doi.org/10.1029/WR013i003p00531

Walling, D. E. (2006). Human impact on land–ocean sediment transfer by the world's rivers. *Geomorphology*, *79*, 192–216. https://doi.org/10.1016/j.geomorph.2006.06.019

Walling, D. E., Owen, P. N., & Leeks, G. J. L. (1998). The role of channel and floodplain storage in the suspended sediment budget of the River Ouse, Yorkshire, UK. *Geomorphology*, *22*, 225–242. https://doi.org/10.1016/S0169-555X(97)00086-X

Walling, D. E., & Webb, B. W. (1981). *The reliability of suspended load data* (IAHS Special Publications No. 133, pp. 177–194). IAHS Press.

Walling, D. E., & Webb, B. W. (1988). *The reliability of rating curve estimates of suspended sediment yield; some further comments* (IAHS Special Publications No. 174, pp. 337–350). IAHS Press.

Wan, G., Yang, M., Liu, Z., Wang, X., & Liang, X. (2017). The precipitation variations in the Qinghai-Xizang (Tibetan) Plateau during 1961–2015. *Atmosphere*, *8*, 80. https://doi.org/10.3390/atmos8050080

Wang, F., Mu, X., Hessel, R., Zhang, W., Ritsema, C., & Li, R. (2013). Runoff and sediment load of the Yan River, China: Changes over the last 60 yr. *Hydrology and Earth System Sciences*, *17*, 2515–2527. https://doi.org/10.5194/hess-17-2515-2013

Wang, Y., Rhoads, B. L., Wang, D., Wu, J., & Zhang, X. (2018). An investigation of the hydrological impacts of large dams on the complexity of suspended sediment dynamics in the mainstream of the Yangtze River. *Journal of Hydrology*, *558*, 184–195. https://doi.org/10.1016/j.jhydrol.2018.01.027

Wang, Z. Y., Li, Y., & He, Y. (2007). Sediment budget of the Changjiang. *Water Resources Research*, *43*, W04401. https://doi.org/10.1029/2006WR005012

Webb, B. W., Phillips, J. M., Walling, D. E., Littlewood, I. G., Watts, C. D., & Leeks, G. J. L. (1997). Load estimation methodologies for British rivers and their relevance to the LOIS RACS(R) programme. *Science of the Total Environment*, *194*, 379–389. https://doi.org/10.1016/S0048-9697(96)05377-6

Webster, P. J., & Hoyos, C. (2004). Prediction of monsoon rainfall and river discharge on 15-30 day time scales. *Bulletin of the American Meteorological Society*, *85*, 1745–1766. https://doi.org/10.1175/BAMS-85-11-1745

Xu, J. (2007). Trends in suspended sediment grain size in the upper Yangtze River and its tributaries, as influenced by human activities. *Hydrological Sciences Journal*, *52*, 777–792. https://doi.org/10.1623/hysj.52.4.777

Xu, J. (2009). Some-rainfall-related thresholds for erosion and sediment yield in the upper Yangtze River basin. *Environmental Geology*, *56*, 1183–1192. https://doi.org/10.1007/s00254-008-1218-z